

**A Theoretical Analysis of the CH₃ + H Reaction:
Isotope Effects, the High Pressure Limit, and Transition State Recrossing**

STEPHEN J. KLIPPENSTEIN,¹ YURI GEORGIEVSKII,¹ and LAWRENCE B. HARDING²

¹*Combustion Research Facility,
Sandia National Laboratories,
Livermore, CA, 94551-0969, USA*

²*Chemistry Division,
Argonne National Laboratory,
Argonne, IL, 60439, USA*

Corresponding author: Lawrence B. Harding

Fax: (630)252-9292

E-mail: harding@anl.gov

Colloquium: Reaction Kinetics of Combustion (Rate-Constants, Free-Radicals)

Word Count: 5439 Total words = 4439 words + 5 Figures * 200 words

Submitted for Oral Presentation

Abstract

The reaction of methyl radicals with hydrogen atoms is studied with a combination of *ab initio* quantum chemistry, variational transition state theory, and classical trajectory simulations. The interaction between the two radicals, including the umbrella mode of the methyl radical, is examined at the CAS+1+2 level using an augmented correlation consistent polarized valence triple zeta basis set. The implementation of an analytic representation of the *ab initio* data within variable reaction coordinate transition state theory yields predictions for the zero-pressure limit isotopic exchange rate constants that are about 15% greater than the available experimental data. Trajectory simulations indicate that the transition state recrossing factor for the capture process is 0.90, essentially independent of temperature and isotope. The dynamically corrected theoretical prediction for the CH₃ + H high pressure rate coefficient is well reproduced by the expression $1.32 \times 10^{-10} T^{0.153} \exp(-15.1/RT) \text{ cm}^3 \text{ molecule}^{-1} \text{ s}^{-1}$, where $R = 1.987 \text{ cal mole}^{-1} \text{ K}^{-1}$, for temperatures between 200 and 2400 K. This prediction is in good agreement with the converted experimental data for all but the one measurement at 200 K. Calculations for the triplet abstraction channel suggest that it is unimportant. Methyl umbrella mode variations have surprisingly little effect on the predicted rate coefficients.

Introduction

The recombination of methyl radicals with hydrogen atoms is of considerable importance in combustion modeling due to the general prominence of both these radicals. Although both the temperature and pressure dependence of this reaction are of importance to combustion modeling, here we shall focus solely on the high-pressure recombination rate coefficient, $k^\infty(T)$ [1]. Due to the difficulty of achieving sufficiently high pressures, particularly at the high temperatures of relevance to combustion, there have been few direct experimental studies of $k^\infty(T)$ for radical-radical reactions.

However, for the $\text{CH}_3 + \text{H}$ reaction, two experimental studies of Pilling and coworkers [2,3] largely circumvented this difficulty by examining the isotopic exchange reactions:



The partially deuterated methane complexes formed during these reactions generally decompose via the loss of an H atom due to the lower zero-point energy of the products. Furthermore, for the $\text{CH}_3 + \text{D}$ reaction the H loss channel is also statistically favored by 3:1. As a result, at room temperature the zero-pressure limit of the $\text{CH}_3 + \text{D}$ reaction rate constant is 92% of that for the corresponding high pressure association [3]. For reactions 2 and 3 the pressure dependence is somewhat greater since their H loss channels are not statistically favored and theoretical models played a somewhat greater role in the conversion from the experimental observations to estimated $k^\infty(T)$ values [3].

Very recently, Su and Michael have also examined the $\text{CH}_3 + \text{D}$ isotope exchange reaction in a shock tube experiment with atomic resonance absorption spectrometric determination of the D atom concentrations [4]. The higher temperatures of this study, i.e., 1294 to 1753 K, also result in a greater deviation between the zero and high pressure limits. Thus, the estimates for $k^\infty(T)$ again rely to some extent on theoretical models for the branching between H and D loss during the decomposition. Furthermore, the conversion from the isotopically substituted $k^\infty(T)$ values to those for the more chemically significant reaction (R1) also requires some model for the isotope effects in the high pressure limit. However, each of these conversions is unlikely to be subject to much error and so these experiments still provide a fairly direct measure of the high pressure rate coefficients.

The data of Su and Michael [4], when combined with the room temperature data of Pilling and coworkers [2,3], provides an important opportunity to test the adequacy of *a priori* theoretical predictions for $k^\infty(T)$. In part due

to its relative simplicity, the $\text{CH}_3 + \text{H}$ recombination has already served as a testing ground for numerous theoretical models (see, e.g., Refs. [5-14]). In many instances, these prior studies yielded results that are in good agreement with this new experimental data. However, the limited nature of the earlier *ab initio* simulations [10,15-18] implies significant uncertainties in the quantitative validity of the resulting potential energy surfaces. Thus, one cannot be certain that the agreement is not the result of a cancellation of errors in the potentials and the dynamical treatments.

The theoretical analysis presented here proceeds beyond these prior analyses in a variety of ways. First, and most importantly, the underlying potential energy surface is evaluated at a much higher level, for a fine grid of relative H atom positions, and with an explicit treatment of the CH_3 radical umbrella mode. We also employ the variable reaction coordinate (VRC) implementation of transition state theory (TST), which allows for a more complete optimization of the transition state dividing surfaces and correspondingly improved predictions for the rate constants. This more complete optimization may also yield differences in the estimated kinetic isotope effects, even for just the addition process, as recently described in Ref. [19]. In addition, rigid body trajectory simulations are used to directly examine the extent of any dynamical effects for the rigid body capture rate. Interestingly, both more standard quasiclassical trajectory simulations [12] and a recent quantum dynamics study [20] suggest that there is some recrossing of the transition state dividing surfaces employed in earlier work, but that this recrossing reduces the rate by about 20% or less. Finally, some consideration is also given to the possible contribution of the triplet abstraction channel:



Theory

A. Potential Surface Calculations

Electronic structure calculations were carried out for both the singlet surface which correlates with ground state CH₄ and the triplet surface which correlates with abstraction products H₂+CH₂(³B₁). At large separations between the reactants, the singlet wavefunction is inherently multi-reference in character while the triplet wavefunction can be well described with single reference methods. For the singlet surface then we use multi-reference configuration interaction (MR-CI) calculations employing orbitals optimized using the complete active space, self-consistent field (CASSCF) methodology. In these calculations, the CASSCF reference wavefunction consists of two active orbitals and two active electrons. This is the minimum necessary to correctly describe the breaking CH bond. The effects of higher order excitations were tested using a multi-reference Davidson correction and were found to be unimportant. The basis set used in all calculations was the correlation-consistent, augmented polarized valence triple zeta (aug-cc-pvtz) basis set of Dunning [21-23]. All calculations were carried out using the COLUMBUS package of codes [24].

For the calculations on the triplet surface we use coupled-cluster, CCSD(T), calculations [25], again with the aug-cc-pvtz basis set. These calculations were carried out using the MOLPRO package [26]. The question to be addressed here is whether or not the abstraction reaction contributes significantly. Unlike the addition reaction on the singlet surface, the abstraction reaction on the triplet surface has a well defined saddle point. The CCSD(T) calculations predict this saddle point to lie 15.3 kcal/mole above the reactants. This is sufficiently high that this pathway will not compete significantly with the barrier-less reaction on the singlet surface. Indeed, a conventional transition state theory estimate, employing rigid rotor harmonic oscillator approximations, suggests that this channel contributes only 4% at 2400 K.

B. Transition State Theory

The VRC-TST formalism is employed in the present calculations of the energy, E , and total angular momentum, J , resolved transition state numbers of states, N_{EJ}^\ddagger , for each isotopic variant of the CH₃ + H addition [27]. The transition state dividing surfaces are defined in terms of a fixed separation r between the H atom, and a pivot point taken to lie along the C₃ axis of the CH₃ fragment, at a distance d from the C atom. The variational

minimization is performed with respect to both the separation r and the distance d , with r ranging from 2.0 to 8.0 Å, and d ranging from 0.0 to 1.2 Å. The optimized d values are generally near 0.8 Å. In contrast, in the flexible transition state theory (FTST) analysis of Ref. 11, the CH₃ pivot point was constrained to be at its center-of-mass, i.e., $d=0$. Here, the contribution from the two separate faces of the CH₃ radical are evaluated separately and added together, as is appropriate for a vibrationally adiabatic (with respect to the motion of the reactive H atom) treatment of the umbrella mode.

Within this formalism the evaluation of N_{EJ}^\ddagger proceeds via an assumed separation of modes, into the vibrational modes of the CH₃ fragment, termed the conserved modes, and the remaining relative and overall rotational modes, termed the transitional modes. The transitional mode contribution to N_{EJ}^\ddagger is evaluated via Monte Carlo integration of classical phase space integrals, with sufficient sampling statistics to reduce the integration error bars to 1% or less. This transitional mode contribution is convoluted with the contribution from the conserved modes, with the latter obtained from a direct quantum sum. The conserved modes are generally treated as harmonic oscillators with the vibrational frequencies obtained from the multi-reference configuration interaction calculations. However, a semiclassical evaluation of the umbrella mode states, including their variation as a function of the H atom position, is also considered here. In each case, the conserved modes are treated in the vibrationally adiabatic limit.

For a spherical top the quantum state degeneracy is $(2J+1)^2$ whereas the classical state degeneracy is $(2J)^2$. Thus, in prior work, we have occasionally applied an ad-hoc semiclassical correction of $(2J+1)^2/(2J)^2$ to the value obtained for N_{EJ}^\ddagger from the classical phase space integral. Here, however, we have determined that the classical and quantum results for a sample isotropic potential are in good agreement, being within 1% at room temperature, while the ad-hoc correction yields results that are 12% too large at room temperature. Thus, no semiclassical rotational correction was applied here. The failure of the ad-hoc semiclassical correction is likely indicative of the need to consider similar corrections to the energies in the phase space integrals (e.g., by replacing BJ^2 with $BJ(J+1)$).

C. Kinetics

The high pressure addition rate constant is evaluated from the expression

$$k_{TST}^\infty(T) = \frac{g_e \sigma}{h \sigma^\ddagger Q_{\text{reactants}}(T)} \int dE dJ N_{EJ}^\ddagger \exp(-\beta E), \quad (1)$$

where g_e is the electronic degeneracy factor of $1/4$, σ and σ^\ddagger are the rotational symmetry numbers for the reactants and the transition state, respectively, $Q_{\text{reactants}}(T)$ is the canonical partition function for the reactants, and $\beta = 1/k_B T$. For the $\text{CH}_3 + \text{D}$ reaction the zero-pressure limit rate constant, $k_0(T)$, is written as [28]

$$k_0^{TST}(T) = \frac{g_e \sigma}{h \sigma^\ddagger Q_{\text{reactants}}(T)} \int dE dJ N_{EJ}^\ddagger(\text{CH}_3 + \text{D}) \exp(-\beta E) \frac{N_{EJ}^\ddagger(\text{CH}_2\text{D} + \text{H})}{N_{EJ}^\ddagger(\text{CH}_2\text{D} + \text{H}) + N_{EJ}^\ddagger(\text{CH}_3 + \text{D})}, \quad (2)$$

which accounts for the probability that the CH_3D adduct decomposes to $\text{CH}_2\text{D} + \text{H}$. Analogous expressions are employed in the evaluation of $k_0(T)$ for the $\text{CH}_2\text{D} + \text{D}$, and $\text{CHD}_2 + \text{D}$ reactions.

D. Trajectory Simulations

Trajectory based estimates for the rate constants are obtained on the basis of a procedure introduced by Keck [29]. This procedure involves propagations forward and backward in time of an ensemble of trajectories initiated at some approximate dividing surface, S , with trajectory weights equal to their contribution to the reactive flux (within TST for the given dividing surface S). With this approach the rate constant is obtained from the expression

$$k_{\text{traj}}^\infty(T) = \langle \chi_{\text{reac}}(q, p; S) \rangle k_{\text{TST}}^\infty(T; S), \quad (3)$$

where the reactivity factor, χ_{reac} , specifies whether the trajectory initiated at phase space point (q, p) on the dividing surface S is reactive or not. Importantly, the final result for the trajectory rate constant is independent of the dividing surface S .

Here, for numerical and programming efficacy, S is taken to be the canonically optimized dividing surface with $d=0$. Also, χ_{reac} is taken to be unity if the forward propagated trajectories reach a CH separation of 2.8 bohr without recrossing S , and the backward propagated trajectories reach a CH separation of 15 bohr without having the CH separation decrease below 2.8 bohr. Otherwise, the recrossing factor is taken to be zero. The initial conditions (q, p) for these trajectories are chosen in a manner that will be described in more detail in a future publication. A total of 10,000 trajectories were propagated for each of the results presented below, which corresponds to sampling error bars of 0.6%.

For these trajectory simulations the CH_3 fragment is treated as a rigid body in direct analogy with the assumed separation of conserved and transitional modes within the transition state theory calculations. This rigid body propagation also removes the possibility of an inappropriate transfer of energy from the zero-point of the

conserved modes to the transitional modes. The final trajectory estimate for the rigid body capture rate constant is then directly comparable to our best E/J resolved VRC-TST estimates (i.e., including the full range of d and r values in the minimization). The ratio of these two numbers is taken to define the recrossing factor for our best dividing surfaces.

Results and Discussion

A. Potential Surface Calculations

$\text{CH}_3 + \text{H}$ is a 12 dimensional problem. Explicit characterization of the full 12 dimensional potential surface is beyond the scope of this work. In order to reduce the dimensionality of the problem we make two constraints: (1) the inactive CH bond lengths are kept fixed, and (2) the CH_3 fragment is required to have C_{3v} symmetry. This leaves four dimensions that will be treated explicitly in these calculations: (1) the active CH distance, R ; (2) a polar angle, θ , defined to be the angle between the nascent CH bond and the C_3 axis of the CH_3 fragment; (3) an azimuthal angle, ϕ , defined to be the dihedral angle between the plane defined by the active H atom and the C_3 axis and the plane defined by the C_3 axis and one of the inactive H atoms; and (4) the umbrella angle, α , of the CH_3 fragment, defined to be the angle between any one of the three inactive H atoms and the C_3 axis. In this $(R, \theta, \phi, \alpha)$ coordinate system, electronic structure calculations were carried out at a rectangular grid of $14 \times 19 \times 6 \times 7 = 11,172$ points (symmetry considerations reduce this number by approximately a factor of 2). The spacings in all of the angle coordinates were 10° and the spacings in the distance coordinate, R , varied from 0.2 to 3.0 au.

The calculated points were then fit to an analytic form in the following manner. First for fixed values of R , θ , and α , the six azimuthal angle, ϕ , energies were fit to six term cosine fourier series, $c_n \cos(3n\phi)$ where $n=0-5$. The resulting Fourier coefficients, c_n , were then fit with three dimensional splines (as functions of R , θ , and α). This then results in an exact fit of all the calculated points.

Two dimensional slices of the surface are shown on the left side of Fig 1. In the bottom plot the methyl radical is planar, while in the top plot the methyl umbrella angle is distorted 30° from planar. For planar methyl radical the top and bottom approaches are, of course, equally attractive. For non-planar methyl this is not true, however, even when the methyl is distorted by 30° from planarity, sufficient to raise its energy by 24 kcal/mole, both approaches are still barrierless.

On the right side of Fig 1 are corresponding plots of the methyl radical orbital, again for both planar and nonplanar geometries. For planar methyl the nodal plane of the radical orbital is, of course, in the plane of the molecule. Note, however, that in the nonplanar plot the nodal plane has not significantly moved. This has an impact on the repulsive part of the long range $\text{H} + \text{CH}_3$ interaction potential. Comparing the planar and nonplanar potential plots we see that the long-range repulsive parts of the potential do not change significantly when the methyl is distorted, indeed the long-range maximum repulsion appears to coincide with the orbital nodal planes. This suggests

that the long-range repulsion is determined more by poor overlap between the two radical orbitals than by non-bonded repulsions between the active hydrogen atom and the existing CH bond of the CH₃ radical. Note that this is true only at long-range. At shorter distances, as can be clearly seen in the upper left plot, the orientation of maximum repulsion coincides with the in-plane, methyl, CH bond.

B. Reaction Kinetics

As illustrated in Fig. 2, the present *a priori* VRC-TST estimated $k_0(T)$ for the CH₃ + D reaction exceeds the experimental measurements [2-4], but only by about 15%. The master equation calculations of Seakins et al. suggest that the pressures employed in the isotope exchange studies should yield rate coefficients that do not deviate significantly from their zero pressure limits [3]. The VRC-TST estimates for $k_0(T)$ at 300 K in the CH₂D + D and CHD₂ + D reactions of 2.06×10^{-10} and 1.46×10^{-10} cm³molecule⁻¹s⁻¹, respectively, also exceed the experimentally measured values of $(1.74 \pm 0.17) \times 10^{-10}$ and $(1.29 \pm 0.09) \times 10^{-10}$ cm³molecule⁻¹s⁻¹ [3] by about 15%. However, for the CHD₂ + D reaction at 200 K Seakins et al. observed a much lower value of $(0.84 \pm 0.04) \times 10^{-10}$ cm³molecule⁻¹s⁻¹ [3], which is a factor of 1.9 lower than the VRC-TST prediction of 1.57×10^{-10} cm³molecule⁻¹s⁻¹.

Predictions for $k^\infty(T)$ in the unsubstituted CH₃ + H reaction are of more importance to combustion models than these $k_0(T)$ values. Thus, we convert the experimental measurements of $k_0(T)$ for reaction (R1) to (R3) to $k^\infty(T)$ values for the CH₃ + H reaction by multiplying by theoretical predictions for (i) the ratio of high and low pressure limits, and (ii) the ratio of isotope effects for the high pressure limit. For the present VRC-TST analysis at room temperature $k_0(T)/k^\infty(T)$ is predicted to be 0.92, 0.79, and 0.58 for reactions (R1), (R2), and (R3), respectively. By comparison the FTST analysis of Seakins et al. [3], based on the Hirst-Hase potential of Ref. [10] and with the pivot point restricted to the center-of-mass of the CH₃ fragment ($d=0$), yielded ratios of 0.92, 0.82 and 0.67. The present decreased predictions for these ratios in (R2) and (R3) ultimately yields improved consistency in the predicted $k^\infty(T)$ from the different isotopic exchange reactions (cf. the data of Seakins et al. in Fig. 3). As expected, for each of these reactions, the ratios are predicted to decrease significantly with increasing temperature, reaching values of 0.79, 0.57, and 0.31, respectively, at 1700 K.

Both the present VRC-TST calculations and the trajectory simulations predict similar small deviations of the high pressure kinetic isotope effects (KIE) from the standard collision frequency ratios. In particular, for the trajectory simulations, the CH₃+H to CH₃+D KIE tends to be about 4% lower than the collision frequency ratio,

while the predicted CH_3+H to CHD_2+D KIE is close to the collision frequency ratio of 1.382. The deviation from the collision frequency for the CH_3+H to CHD_2+D KIE tends to be between the other two.

The purely theoretical predictions for $k^\infty(T)$ for the $\text{CH}_3 + \text{H}$ reaction are plotted together with the converted experimental values in Fig. 3. The consistency of the experimentally based estimates from Ref. [3], aside from the one 200 K result, suggests that the present transition state theory analysis provides an adequate conversion from the isotopic exchange rate constants. The averaged room temperature experimental $k^\infty(T)$ from Refs. [2] and [3] are 2.6×10^{-10} and $3.0 \times 10^{-10} \text{ cm}^3 \text{ molecule}^{-1} \text{ s}^{-1}$, respectively. The fully optimized E/J resolved VRC-TST results again are only slightly greater than the experimental values. The trajectory simulations yield a recrossing factor of 0.91 for the $\text{CH}_3 + \text{H}$ addition reaction and about 0.89 for the D additions, all essentially independent of temperature. Correcting the VRC-TST results by this recrossing factor yields *a priori* estimates that are well represented in the 200 to 2400 K range by the expression $1.32 \times 10^{-10} T^{0.153} \exp(-15.1/RT) \text{ cm}^3 \text{ molecule}^{-1} \text{ s}^{-1}$ ($R=1.987 \text{ cal mole}^{-1} \text{ K}^{-1}$), and which generally deviate from the experimental results by an amount that is on the order of the experiments statistical error bars.

These theoretical predictions for the association rate constant can be converted to corresponding predictions for the dissociation rate constant via the equilibrium constant. Doing so yields rate coefficients that are three times greater than the predictions of Stewart et al. [30] near 1000 K, obtained via extrapolation of the pressure dependent data of Chen et al [31]. This deviation may simply be indicative of the uncertainties in extrapolating to the high-pressure limit.

It is instructive to compare the present high-level theoretical results with results from simpler, less computationally demanding theories. The present calculations agree well with the Lennard-Jones model presented by Su and Michael [4] although the Lennard-Jones model predicts slightly more T dependence. To compare to Gorin models [32] one must make an assumption regarding the hindrance or steric factor. If one treats the hindrance as an adjustable parameter, as is commonly done, we find excellent agreement (to within a few percent) between our calculations and a Gorin model with no hindrance. Alternatively one can attempt to extract a hindrance parameter from the present calculations. One way to do this is to replace the anisotropic potential with an isotropic potential whose energy, as a function of R , equals the ab initio energy along the minimum energy path. This removes all the repulsive parts of the potential. We then define the steric factor to be the ratio of the rate calculated with the full potential to the rate calculated with the isotropically attractive potential. Defined in this way the steric factor ranges

from 0.8 at 300°K to 0.6 at 2000°K. So, although there is remarkably good agreement between the present calculations and a zero-hindrance Gorin model, this may be due in part to a cancellation of different effects.

Also plotted in Fig. 3 are the results of VRC-TST calculations employing the Hirst-Hase potential of Ref. [10]. The results from these calculations are reasonably representative of the large number of prior theoretical studies employing this potential [3,10-12]. Rigid body trajectory simulations for the Hirst-Hase potential yield a recrossing factor that is similar to that calculated for the present higher level potential. The deviations between the VRC-TST results for these two potentials are indicative of the significant differences between the two potentials. The present potential is substantially more attractive along the minimum energy path (e.g., by about 60% at $R = 3.2$ Å, where the present potential is -2.4 kcal/mol), which correlates with a substantial increase in the predicted rate constants. However, this increased attractiveness is partly ameliorated by the increased repulsiveness in the present potential for approach in the CH_3 plane, as can be seen from comparison of the contour plot for the Hirst-Hase potential provided in Fig. 4, with that in Fig. 1. The present use of higher levels of configuration interaction, a substantially larger basis set, and the generation of a much finer grid of data implies that the present potential and corresponding kinetics predictions should be considered as much more reliable.

The effect of considering d values different from 0 in the minimization of the TST predictions for $k^\infty(T)$ is small but significant. In particular, this consideration reduces the rate constant by 0.93 at 200 K. This factor gradually decreases with increasing temperature, reaching 0.85 at 850 K, at which point it becomes temperature independent. These reductions are similar to those calculated by Mardis and Sibert in their quantum dynamics study of the cumulative reaction probability for $\text{CH}_3 + \text{H}$ in $J=0$. However, the above trajectory analysis indicates that the best VRC-TST dividing surfaces have not removed all of the recrossing.

The properties of the CH_3 umbrella mode change quite substantially during the association and one might expect this variation to have a significant effect on the kinetics. Notably, a semiclassical vibrational analysis with the present potential yields transition frequencies of 615, 693, and 750 cm^{-1} for the first three levels, which are within 1-3% of the experimentally measured values of 607, 682, and 731 cm^{-1} [33]. However, the umbrella mode variations have only a very minor effect on the rate constant predictions. In particular, the decrease in the potential energy arising from the relaxation of the umbrella mode angle yields at most a 4% increase in the VRC-TST predictions for temperatures below 2400 K. Meanwhile, incorporating the changes in the umbrella mode zero-point energy and vibrational energy levels reduces the predicted rate constant by 2% or less. As illustrated in Fig. 5, while

the changes in the umbrella mode energies are substantial, the transition state tends to lie just beyond the region where the umbrella mode vibrational partition function decreases from its free CH₃ value. Thus, for the present reaction, the effect of the variation in the conserved modes can be safely ignored. For other reactions, the conserved mode variations have been more significant, but the two effects (i.e., energy relaxation and frequency variation) do tend to cancel. The Hirst-Hase potential similarly yields a negligible effect for the vibrational energy level changes while the energy relaxation is somewhat greater yielding an increase of about 13% at room temperature.

Summary

A combination of MR-CI *ab initio* simulations, VRC-TST calculations, and rigid body trajectory simulations are applied to the analysis of the high pressure limit of the CH₃ + H recombination reaction and the related zero-pressure isotopic exchange reactions. The potential energy surface arising from these MR-CI calculations differs significantly from the Hirst-Hase potential commonly used in prior studies. The dynamically corrected VRC-TST results for the CH₃ + H high pressure recombination rate constant are in good agreement with the available experimental results. In the 200 to 2400 K range these theoretical predictions are well reproduced by the expression $1.32 \times 10^{-10} T^{0.153} \exp(-15.1/RT) \text{ cm}^3 \text{ molecule}^{-1} \text{ s}^{-1}$, where $R = 1.987 \text{ cal mole}^{-1} \text{ K}^{-1}$. Over the 300 to 2000 K range, this expression yields an increase by a factor of 1.29. The dynamical correction factor of 0.90 is close to unity, illustrating the reasonable accuracy of the VRC-TST calculations. The good agreement between theory and experiment for prior calculations with the Hirst-Hase potential is due in part to the cancellation of errors in different aspects of the potential and in the kinetic models. The triplet channel is predicted to make a negligible contribution to the kinetics.

Acknowledgments

We would like to thank M.-C. Su and J. V. Michael for providing us with their data prior to publication. This work was supported by the U. S. Department of Energy, Office of Basic Energy Sciences, Division of Chemical Sciences, Geosciences, and Biosciences (at Argonne under DOE Contract Number W-31-109-ENG-38).

References

- (1) A detailed analysis of the low pressure limit will be provided in a separate article: Miller, J. A., and Klippenstein, S. J., *J. Phys. Chem. A*, in press (2001).
- (2) Brouard, M., Macpherson, M. T., and Pilling, M. J., *J. Phys. Chem.* 93: 4047 (1989).
- (3) Seakins, P. W., Robertson, S. H., Pilling, M. J., Wardlaw, D. M., Nesbitt, F. L., Thorn, R. P., Payne, and W. A., Stief, L. J., *J. Phys. Chem. A*, 101:9974-9987 (1997).
- (4) Su, M.-C., and Michael, J. V., *Proc. Comb. Inst.*, 29, submitted (2001).
- (5) Wardlaw, D. M. and Marcus, R. A., *Chem. Phys. Lett.*, 110:230 (1984); *J. Chem. Phys.* 83: 3462 (1985).
- (6) Duchovic, R. J., and Hase, W. L., *Chem. Phys. Lett.*, 110: 474 (1984); *J. Chem. Phys.* 82: 3599 (1985); *J. Chem. Phys.* 83:3448 (1985).
- (7) Cobos, C. J., and Troe J., *Chem. Phys. Lett.*, 113: 419-424 (1985); Cobos, C. J., *J. Chem. Phys.*, 85:5644-5651 (1986).
- (8) Viswanathan, R., Raff, L. M., and Thompson, D. L., *J. Chem. Phys.* 82:3083 (1985).
- (9) R. J., Leblanc, J. F., and Pacey, P.D., *J. Chem. Phys.*, 83:4511-4515 (1985); King, S. C., Leblanc, J. F., and Pacey, P. D., *Chem. Phys.*, 123: 329-338 (1988); Furue, H., Leblanc, J. F., Pacey, P. D., and Whalen, J. M., *Chem. Phys.*, 154: 425-435 (1991).
- (10) Hase, W. L., Mondro, S. L., Duchovic, R. J., and Hirst, D. M., *J. Am. Chem. Soc.* 109: 2917 (1987).
- (11) Aubanel, E. E., and Wardlaw, D. M., *J. Phys. Chem.* 93:3117 (1989).
- (12) Hu, X., and Hase, W. L., *J. Chem. Phys.* 95:8073 (1991).
- (13) Forst, W., *J. Phys. Chem.* 95: 3612-3620 (1991); *Chem. Phys. Lett.*, 194: 21-26 (1992).
- (14) Naroznik M., and Niedzielski J., *J. Chem. Soc. Faraday Trans.*, 94:2541-2547 (1998).
- (15) Duchovic, R. J., Hase, W. L., Schlegel, H. B., Frisch, M. J., and Raghavachari, K., *Chem. Phys. Lett.*, 89: 120 (1982).
- (16) Brown, F. B., Truhlar, D. G., *Chem. Phys. Lett.* 113:441 (1985).
- (17) Hirst, D. M., *Chem. Phys. Lett.* 122:225 (1985).
- (18) Schlegel, H. B., *J. Phys. Chem.* 84:4530 (1986).
- (19) Taatjes, C. A., Klippenstein, S. J., *J. Phys. Chem. A* 105:8567-8578 (2001).

- (20) Mardis, K. L., Sibert, E. L. III, *J. Chem. Phys.* 109:8897-8906 (1998).
- (21) Dunning, T.H., Jr., *J. Chem. Phys.* 90:1007-1023(1989).
- (22) Kendall, R.A., Dunning, T.H., Jr., Harrison, R.J., *J. Chem. Phys.* 96:6796-6806 (1992)
- (23) Woon, D.E., and Dunning, T.H. Jr., *J. Chem. Phys.* 98:1358-1371 (1993).
- (24) Shepard, R., Shavitt, I., Pitzer, R.M., Comeau, D.C., Pepper, M., Lischka, H., Szalay, P.G., Ahlrichs, R., Brown, F.B., and Zhao, J.-G. *Int. J. Quantum Chem.* S22:149-165 (1988).
- (25) Hampel, C., Peterson, K., and Werner, H.-J. *Chem. Phys. Lett.* 190:1 (1992) and references therein.
- (26) MOLPRO is a package of ab initio programs written by Werner, H.-J. and Knowles, P. J. with contributions from Almlöf, J., Amos, R. D., Berning, A., Cooper, D. L., Deegan, M. J. O., Dobbyn, A. J., Eckert, F., Elbert, S. T., Hampel, C., Lindh, R., Lloyd, A. W., Meyer, W., Nicklass, A., Peterson, K., Pitzer, R., Stone, A. J., Taylor, P. R., Mura, M. E., Pulay, P., Schutz, M., Stoll, H., Thorsteinsson, T.
- (27) Klippenstein, S. J., *J. Chem. Phys.* 94: 6469 (1991); *ibid.* 96: 367 (1992); *J. Phys. Chem.* 98: 11459 (1994).
- (28) Miller, W. H., *J. Chem. Phys.* 65: 2216 (1976).
- (29) Keck, J. C., *Adv. Chem. Phys.* 13:85 (1967).
- (30) Stewart, P. H., Smith, G. P., and Golden, D. M., *Int. J. Chem. Kinet.* 21: 923 (1989).
- (31) Chen, C.-J., Back, M.H., Back, R. A., *Can. J. Chem.* 53: 3580 (1975).
- (32) Gorin, E., *J. Chem. Phys.* 7: 256, 633 (1939); Benson, S. W., *Can. J. Chem.* 61: 881 (1983).
- (33) Yamada, C., Hirota, E., Kawaguchi, K., *J. Chem. Phys.* 75:3256 (1981).

Figure Captions:

Fig. 1. Two dimensional plots of the $\text{H}+\text{CH}_3 \rightarrow \text{CH}_4$ potential surface, V , and of the CH_3 radical orbital, χ_{rad} . The plotting planes contain the C_3 axis and one of the inactive CH bonds. Solid contours are positive, dashed contours negative and the zero energy contour (defined to be the energy of the $\text{H}+\text{CH}_3$) is shown with a heavy solid line. The energy contour increment is 5 kcal/mole and all distances are shown in atomic units (one atomic unit = 0.52918 Å).

Fig. 2. Plot of the temperature dependence of the VRC-TST prediction for the $\text{CH}_3 + \text{D}$ zero-pressure isotopic exchange rate constant, together with the experimental data [2-4].

Fig 3. Plot of the temperature dependence of various theoretical and experimental results for the high pressure limit of the rate coefficient for the recombination of CH_3 with H. The solid and dashed lines denote the present VRC-TST and trajectory results for the present MRCI based potential, and the dotted line the present VRC-TST results for the Hirst-Hase potential [10].

Fig. 4. Two dimensional plot of the $\text{H} + \text{CH}_3$ potential from Ref. [10]. The methyl radical is kept planar. Other plotting conventions are as in Fig 1.

Fig. 5. Plot of the changes in the conserved mode canonical partition function with CH separation R along the minimum energy path for three temperatures (the dashed, the dotted, and the dashed-dotted are for 300, 1000, and 2000 K, respectively). The solid line denotes the analogous change in the zero-point energy. The solid dots denote the CH separation at the canonical transition state dividing surface (with d constrained to 0) for $T=2000, 1000,$ and 300, from left to right.

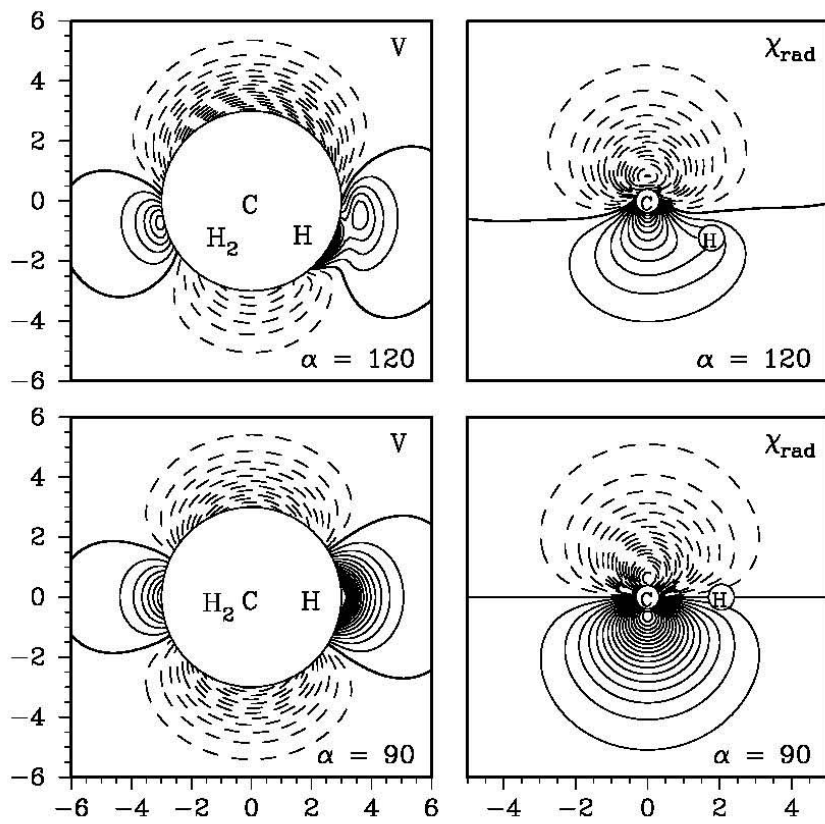


Fig.1

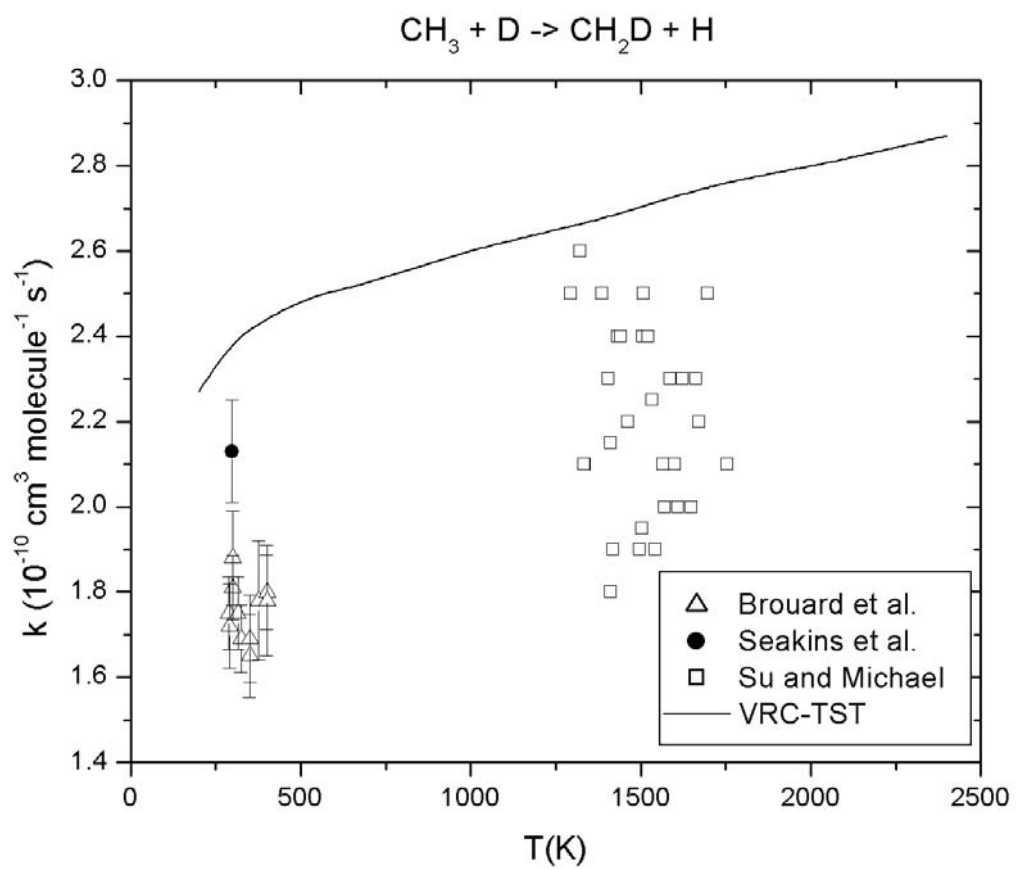


Fig. 2

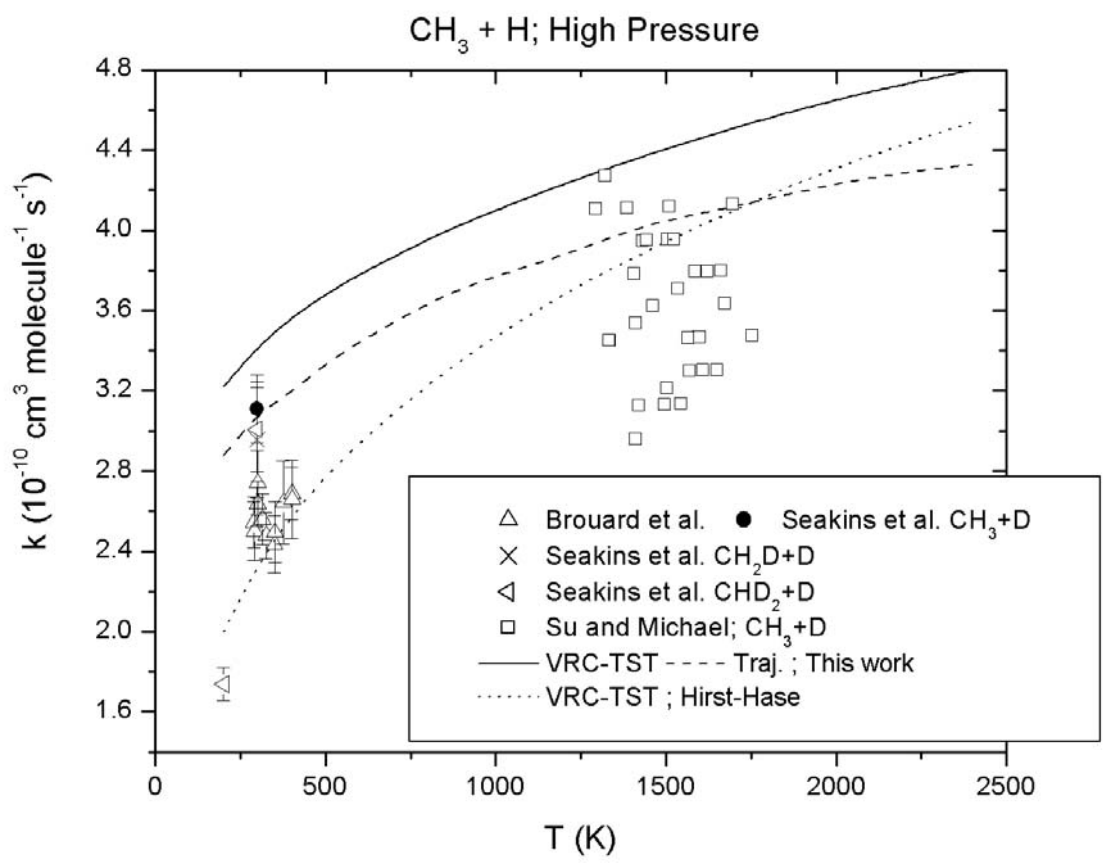


Fig. 3

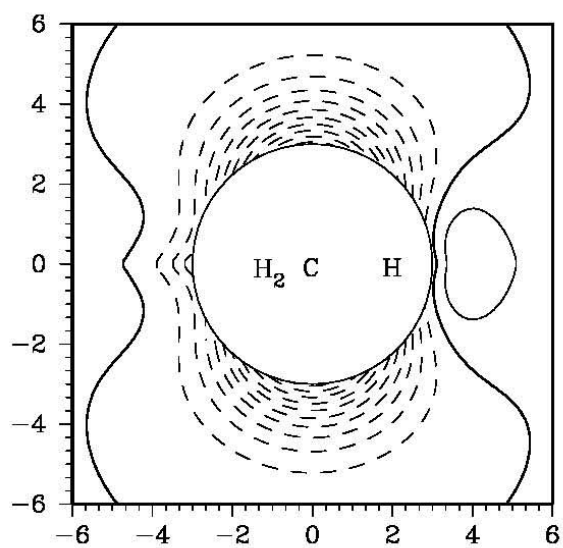


Fig. 4

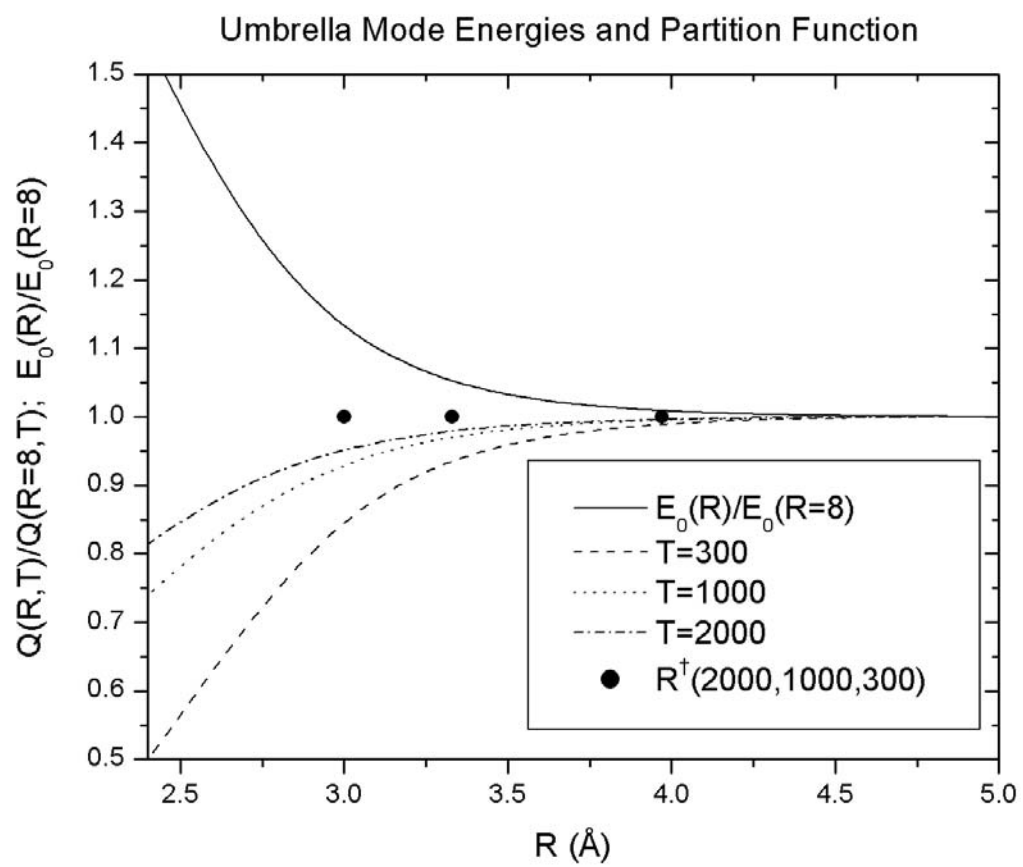


Fig. 5